A CFD ANALYSIS OF THE 14-BIS AIRCRAFT AERODYNAMICS

Ramon M. Freitas* , **Leonardo O. Bitencourt**** , **Grégori Pogorzelski**** , **João L. F. Azevedo*****
* **Instituto Nacional de Pesquisas Espaciais, INPE**
** **Instituto Tecnológico de Aeronáutica, CTA/ITA/IEA**
*** **Instituto de Aeronáutica e Espaço, CTA/IAE/ASA-L**

Keywords: *Aerodynamics, CFD, Centennial of Flight, Santos Dumont, 14-Bis*

Abstract

The year 2006 marks the centennial of the historical, heavier-than-air flight by Alberto Santos Dumont with his 14-Bis aircraft. This aircraft had a complex canard-biplane configuration, based on Hargrave's box kites. In this context, the present work describes the results of a CFD-based analysis of the 14-Bis aircraft aerodynamics and flight stability. The 14-Bis aircraft CAD geometry was generated from historical sources and observations. CFD computations are performed using well-established commercial codes for calculation of the historical flight conditions. The computations consider a Reynolds-averaged Navier-Stokes formulation, in which turbulence closure is achieved using Menter's SST model. The calculations consider unstructured grids and the codes feature a multigrid method for convergence acceleration. The flight conditions investigated are primarily concerned with historical observations regarding flight speeds and the need for a more powerful engine, as well as flight stability characteristics of the 14-Bis airplane, which are unknown up to the present day. The results lead to qualitative agreement with historical reports, although quite interesting conclusions can be drawn with regard to actual aerodynamic flight speeds and aircraft stability parameters.

1 Introduction

On October 1906, in the Bagatelli Field, Paris, France, Santos Dumont flew the 14-Bis aircraft and won the Deutsch-Archdeacon Prize for the first officially observed heavier-than-air powered flight. The 14-Bis was constructed from pine and bamboo poles covered with Japanese silk. The aircraft had a complex canard-biplane configuration, which was a construction based on Hargrave's box kites. The Hargrave cell in the nose pivoted up and down to act as an elevator and from side to side in the role of a rudder. The wings were rigged with 10 deg. of dihedral and the first flights were made without ailerons. The preliminary flight tests happened with the 14-Bis held by the No. 14 dirigible.

The 14-Bis flew without the dirigible on September 13, 1906, making a hop between 6 and 13 meters. The original power plant was a 24 hp Antoinette engine, but this was upgraded to the 50 hp engine on the October 23 flight, when Santos Dumont managed to fly 60 meters (Fig. 1). Then, on November 12, flying 220 meters in 21 1/2 seconds, with members of the Aero-Club de France in attendance, he won a prize of 1500 francs for making the first flight in Europe over 100 meters. Since he was observed by officials from what would become the Federation Aeronautique Internationale, Santos Dumont was credited with making the first heavier-than-air powered flight [1]. The main 14-Bis geometric characteristics are presented in Table 1.

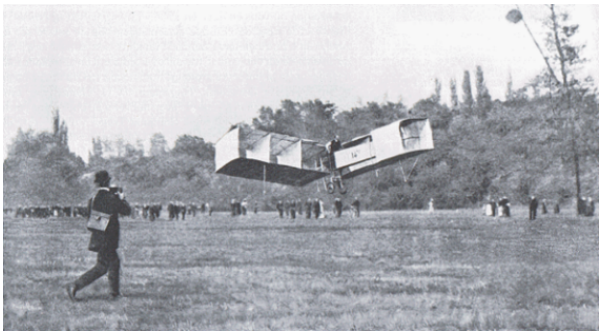

Fig. 1 14-Bis in flight on 23 October 1906 - Source: Museu Aeroespacial, Rio de Janeiro, Brazil.

During a long time, there were only two approaches for aerodynamic studies, wind tunnel testing and analytical solution of simplifications to the Navier-Stokes equations. The last method is very limited, since only some simple cases can be predicted with acceptable accuracy. The wind tunnel also has some disadvantages, such as higher energy consumption and a considerably large time spent constructing the model, performing the tests, and processing the data. Moreover, only some flow conditions can be reproduced. It must be pointed that those factors together are related to more costs.

The computational fluids dynamics (CFD) techniques emerge as an alternative able to reduce project costs, since time and money spent with wind tunnel testing are substantially reduced. In addition to this, CFD has the advantage of numerically solving the fluid equations in the entire flowfield, thus allowing for local analysis of the flow properties in a way much more detailed than any wind tunnel visualization techniques could show. In this context, the main objective of this article is to apply CFD techniques for aerodynamic analysis of the 14-Bis aircraft.

The central idea is to compute lift and drag curves for the 14-Bis aircraft, at the presumed flight conditions, and then assess and clarify some controversial points regarding stability, flight speed, ground effect and power plant performance. The study will also explore angle of attack and velocity variations around the historical data.

Table 1 14-Bis geometric characteristics.

Total Canard Area	8 m^2
Canard Chord	2 m
Canard Span	2 m
Length	10 m
Wing Chord	2.5 m
Wing Span	11.50 m
Historical Flight Speed	9 to 12 m/s
Wing Chord Re	10^7
Wing Dihedral	10 deg.
Canard Chord Re	10^7
Total Wing Area	50 m^2
Canard-Wing Distance	5 m
Weight with Pilot	$\approx$ 300 kg
Engine Power	24 hp(first) - 50 hp

2 Theoretical Formulation

The Navier-Stokes equations constitute the more general flow formulation for which the fluid continuum hypothesis can be assumed. The Navier-Stokes equations, for a perfect gas, without the generation of heat and with negligible field forces can be written as

$$\frac{\partial \rho}{\partial t} + \frac{\partial (\rho u_j)}{\partial x_j} = 0 \,, \tag{1}$$

$$\frac{\partial (\rho u_i)}{\partial t} + \frac{\partial (\rho u_i u_j)}{\partial x_j} + \frac{\partial p}{\partial x_i} - \frac{\partial \tau_{ij}}{\partial x_j} = 0 \,, \tag{2}$$

$$\frac{\partial e}{\partial t} + \frac{\partial [(e+p)\, u_j - \tau_{ij}\, u_i + q_j]}{\partial x_j} = 0 \,, \tag{3}$$

where ρ, p and $\vec{u}$ are the fluid density, pressure and velocity, respectively, $\vec{\vec{\tau}}$ is the viscous stress tensor, $\vec{q}$ is the heat flux vector and t is the time. The e term is the total energy per unit of volume, given by

$$e = \rho \left[e_i + \frac{1}{2} \left(u^2 + v^2 + w^2 \right) \right] \,, \tag{4}$$

where u, v and w are the velocity vector Cartesian components and e_i is the internal energy.

In the formulation actually solved in the present work, two additionl assumptions are adopted: the absence of heat transfer, *i.e.*, the heat flux vector terms equal to zero, and the flow is treated as imcompressible due to the low Mach number values here considered (lower than 0.05). Furthermore, since turbulent effects can be important in the present case, flow analysis is performed using the Reynolds-averaged Navier-Stokes equations. These equations contain the mean variables and a certain number of terms representing the turbulence effects that must be modeled. Turbulence closure is achieved using the SST model [2].

3 Numerical Approach

3.1 Flow Solver

The computations on unstructured grids have been carried out using the CFX code [3], which is a well-known commercial code currently available. The solutions of the turbulent flows of interest are based on the Reynolds-averaged Navier Stokes equations (RANS), supported by Menter's SST turbulence model [2].

In the present case, the CFX solver simulated steady, viscous and incompressible flows around the 14-Bis model. This code uses a cell-vertex, finite element-based control volume method. An iterative, second order, time marching scheme is used to numerically solve the RANS equations. To decrease the computational time, some convergence acceleration techniques, such as an algebraic multigrid (MG) procedure, and parallel computations are used in the simulations.

3.2 Grid Generation

The 14-Bis CAD geometry is generated from planform and historical source observations [4]. The authors have tried to express the real forms of the airplane as much as possible. The flow domain about the geometry is discretized using unstructured grids. Since memory and processing capabilities are limited, the geometry is simplified keeping only the main components, *i.e.*, wings, canard and fuselage. Figures 2, 3 and 4 show a parallel between the original geometry and the simulated one.

The grid generator software used, ICEM-CFD [5], allows the automatic generation of the hexahedral grid. However, the resulting surface mesh over the airplane has a poor arrangement. Then, the strategy adopted is to first create a structured 2-D grid over the geometric surface. Afterwards, the Delauney method [6] is applied, generating the desired unstructured volumetric grid. To assure a faster convergence and a good solution, the mesh quality must be taken into account. Therefore, the element size transitions are performed gradually. Furthermore, regions of leading edges, trailing edges and the ones containing wakes receive appropriate grid refinement to avoid spurious solutions.

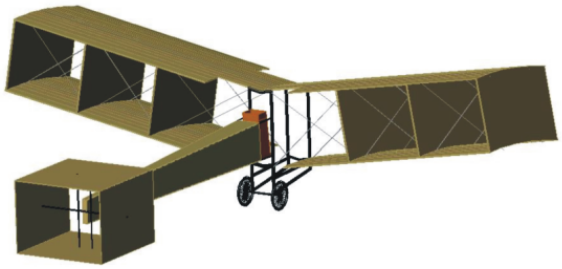

Fig. 2 Original CAD model (Source: EESC-USP).

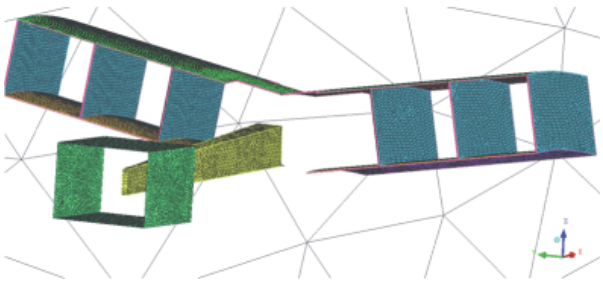

Fig. 3 Mesh view of idealized configuration.

3.3 Boundary Conditions

The correct application of boundary conditions is vital to properly close the numerical problem, as-

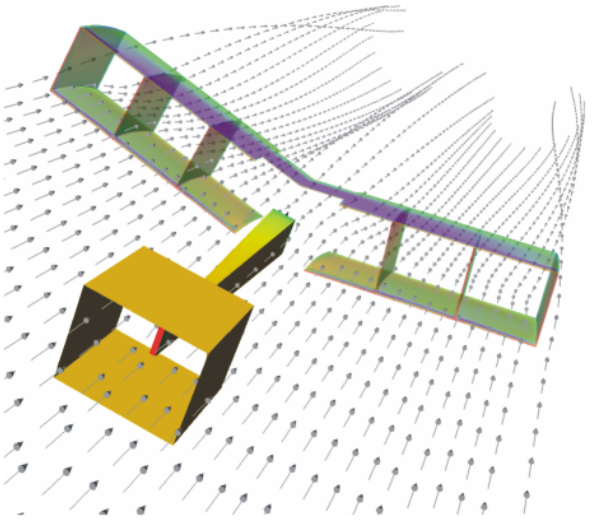

Fig. 4 14-Bis CFD model with streamlines

suring correct modeling. The INLET condition is applied along the computational domain entrance surface. In this boundary, the freestream speed and its direction are specified. The NO-SLIP WALL condition is used in the aircraft surface, as usual for a viscous simulation, and it assures that neither tangential nor normal velocity components are present along the airplane surfaces. The OUTLET condition is used to model the fluid flow at the domain exit. In the simulations here performed, the atmospheric pressure is specified as exit pressure at this particular domain boundary. The SLIP WALL condition is used on the surface just below the airplane in order to model the ground effect. It should be observed that the normal velocity component is kept zero under this condition. Finally, the OPENING condition models a boundary condition which allows entrance and exit of fluid freely. This boundary condition is used for all other external boundary surfaces of the computational domain. It should also be pointed out that the atmospheric pressure is also specified for such boundaries. The nomenclature use here is the one adopted by the CFX solver.

3.4 Post-Processor for Aerodynamics Forces

The post-processor, by means of simple and useful tools, allows evaluation of aerodynamics forces and the observation of the flow field variables as, for example, pressure contours, streamlines (Fig. 4) or boundary layer velocity profiles. The resultant force in the airplane, when projected into the wind axis results in drag, lift and yaw force components. The evaluation of these aerodynamic forces is performed by integrating the surface pressure distributions and shear stresses as shown in Eq. (**??**). A more detailed description of these force integration methods can be found in Ref. [7].

$$\vec{F}_{near} = \int_{S_{near}} \left[(p - p_\infty)\vec{\vec{I}} - \vec{\vec{\tau}} \right] .\vec{n} dS \quad . \qquad (5)$$

The aerodynamic drag is a force exerted by the flowfield on the body surface in a direction contrary to its movement. The drag is the summation of the tangential or skin friction forces, and surface pressure or normal forces, projected into the freestream direction. The drag breakdown with the near-field drag computation approach, as described in Ref. [7], comprises the pressure and the friction drag components.

Evaluating forces and moments over the airplane for several flight conditions, *i.e.*, varying the angle-of-attack or the canard angle, the authors are able to extract the relevant aerodynamics coefficients. With such data, one can analyze details of the 14-Bis flight conditions and possible stability range. The aerodynamic coefficients evaluated in the present work are only valid for small angles-of-attack because, since steady flow conditions are assumed, the calculations beyond stall would be incorrect.

4 Test Cases

The chosen test cases explore the main aerodynamics characteristics of the 14-Bis airplane. Basically, this parametric study includes 46 simulations, involving five major objectives, namely:

- To verify the speed influence over the aerodynamic coefficients;
- To verify the overall aerodynamic behavior at different angles-of-attack and to determine the drag polar;

- To analyze the canard deflection influence over the aircraft;
- To study the aircraft aerodynamics when submitted to sideslip angles;
- To verify the extent of the ground effect.

Velocity variation studies allow the verification that aerodynamic coefficients do not change with the flow speed. Moreover, such studies also allow finding the most probable flight speed, which is not exactly known because historical sources are not in agreement. Through the angle of attack variation studies, it is possible to estimate lift, drag and moment derivatives. The canard incidence angle variation allows the estimation some stability derivatives. Moreover, ground effect influence is checked out varying the distance from the airplane to the ground. All the historical registries only take into account the airplane velocity relative to the ground, but it would be more interesting, in an aerodynamic point of view, to obtain the wind relative velocity. Hence, a range of velocities are tested. The interference between the main airplane parts is also checked.

5 Results and Discussion

5.1 General Aerodynamic Results

The first set of simulations performed has the objective of verifying the influence of the flight speed over the aerodynamic coefficients. As it is well known, for low speed subsonic flight, the general aerodynamic characteristics of an aircraft must have a weak dependence on the flight velocity. Table 2 shows the results concerning the longitudinal aerodynamic coefficients to 4 different simulated speeds: 7.5, 9.5, 11.5 and 14 m/s. The other important flight parameters, namely angle of attack, sideslip angle and elevator deflection are set to 0 deg.

The results of Table 2 show maximum relative differences of 0.29%, 2.48% and 6.35% for C_L, C_D and C_M, respectively, in the speed range analyzed. The relatively small difference values encountered indicate that the aerodynamic coefficients can be treated as independents of the flight velocity. This is further supported by the fact that the range of aerodynamic coefficient variations are probably inside the uncertainty range induced by the model geometrical simplifications adopted as, for example, the ignored aircraft elements, such as the wheels, which certainly would increase the drag coefficient. Therefore, in the following analyses and discussions, the consideration of aerodynamic coefficient independence with respect the flight speed is adopted. This is especially important when a linear aerodynamic model of the aircraft is developed and applied with constant control and stability derivatives over different flight speed values.

Table 2 Longitudinal aerodynamic coefficients at different flight speeds.

Speed (m/s)	C_L	C_D	C_M
7.5	0.8501	0.1002	-0.0606
9.5	0.8511	0.0988	-0.0623
11.5	0.8516	0.0979	-0.0632
14	0.8526	0.0977	-0.0645

The following simulations are concerned with the aerodynamic characteristics of the aircraft under an angle of attack variation with no canard deflection. The flight speed of 11.5 m/s is adopted as the default value for such simulations, because this is the closest value to the reported historical flight speed. A range of angles of attack, varying from -5.0 to 6.5 deg., is considered. The presence of nonlinear effects, probably related to the growth of the separated regions, together with time and computational resource constraints did not allow the exploration of the flow under higher angles of attack. Figure 5 shows the lift coefficient behavior as a function of angle of attack. As can be noted, a general linear pattern is observed, except maybe for the last 2 points, where some nonlinear effects might be beginning to appear. From the results of Figure 5, the value of the $C_{L\alpha}$ derivative can be extracted yielding $C_{L\alpha} = 4.85$ rad^{-1}.

The aircraft drag polar is shown in Fig. 6. To analytically represent the data, a polynomial

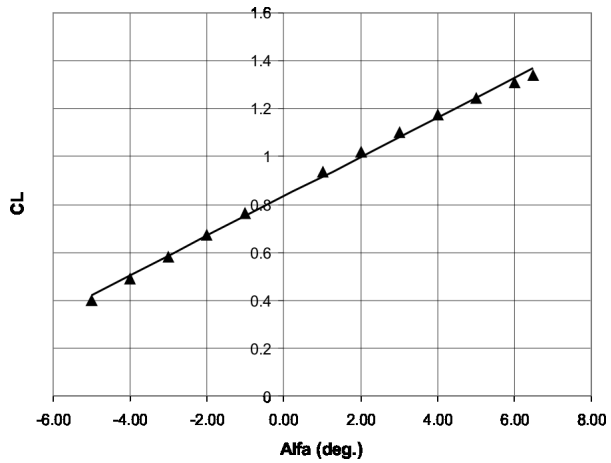

Fig. 5 Aircraft $C_L \times \alpha$ curve. Reference area: $S_{ref} = 28.75$ m^2.

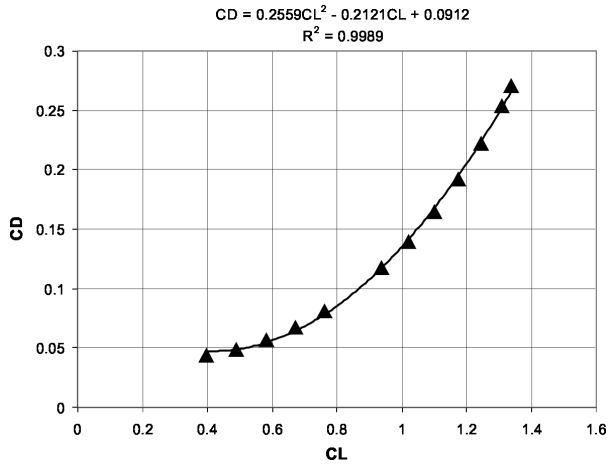

Fig. 6 Aircraft drag polar.

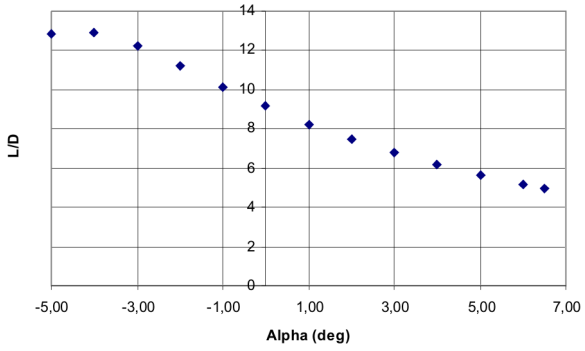

Fig. 7 Aircraft L/D curve.

curve fit of second degree is fitted to the data points. As indicated in the figure, the polynomial is a good approximation and it is adopted as the drag polar model. An important observation, that must be addressed with respect to the drag polar and the general drag results obtained, is concerned with the geometric simplifications assumed in the simulated model. One can expect the missing components, such as struts, landing gear and even the pilot, should increase the drag when compared to the current calculations. Nevertheless, it is hoped that the computational drag polar still gives enough information to a first analysis of the airplane, allowing reasonable drag predictions when simulating the historical flight conditions.

The aerodynamic efficiency behavior at different angles of attack can be seen in Fig. 7. A considerable loss of efficiency can be observed as the angle of attack increases. For instance, a variation of 61% in the L/D values is found between the two extreme points represented. The explanation for such behavior can be found in Figs. 5 and 6. In other words, whereas C_L grows linearly with the angle of attack, the drag coefficient increases significantly after C_L values of approximately 0.6, that corresponds to an angle of attack of -3 deg. (see Fig. 5). In fact, in Fig. 7, one can verify that, for angles of attack higher than 3 deg., L/D values are quite reduced due to, most probably, the fairly large induced drag produced by the aircraft.

It is estimated in Ref. [1] that the 14-Bis aircraft first flight speed was about 11.5 m/s. It must be pointed out that this is a mean speed value using the ground as reference. The wind influence over the airplane speed is not considered. Therefore, the aerodynamic speed could be different from the historical measured value of 11.5 m/s. In addition to that, there is also the speed variation during the acceleration procedure. From all of this information, it is possible to conclude that the true air speed could actually have been higher than the estimated mean value. With the objective of having a better estimative of the most probable speed value, a parametric analysis of this variable influence over the aircraft lift and drag is performed.

According to Ref. [4], the aircraft mass was about 300 kg. Therefore, a lift force higher than 3000 N must have been generated to allow the flight. Figure 8 presents the angle of attack necessary to allow sustained flight for each flight speed. From this figure, it is possible to verify that the minimum lift is reached with speeds of 14.5 and 11.5 m/s, for 0 and 5 deg. of angle of attack, respectively.

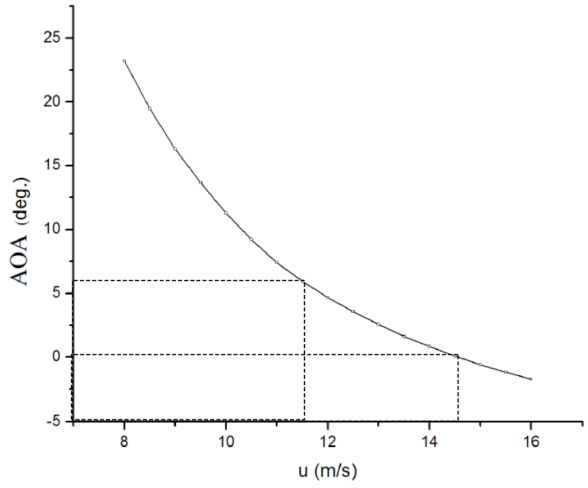

Fig. 8 AoA and flight speed necessary to allow sustained flight.

However, another important parameter that should be analyzed in order to define the flight envelope is the thrust availability. In other words, as the drag force varies as a function of aerodynamic speed, the required force to balance drag must be available from the aircraft engine, using the propeller capability to transform the shaft power into traction. Historical sources, cited by Ref. [1], indicate that Santos Dumont initially used a 24 hp nominal power engine. The power deficiency of this engine became evident on September 1906 during a flying attempt, when the aircraft, in spite of some jumps, was unable to take off. During the following experiments, a new and more powerful engine was selected. Its nominal power was 50 hp at 1500 rpm.

The 14-Bis performance in terms of propulsive efficiency (η_p) is unknown. However, it is important to note that the thrust produced by the engine varies with flight speed, decreasing with the speed increment. As the blades do not completely convert the given engine shaft power into thrust, three isolines of different η_p, namely 20 %, 30 % and 40 %, are considered in the current paper. Figures 9 and 10 indicate the results of such analysis, respectively, for the 24 hp and 50 hp engines. The figures show the drag dependence with speed, and hence the required thrust dependence with speed, and the three available thrust curves considering the different assumed propulsive efficiencies.

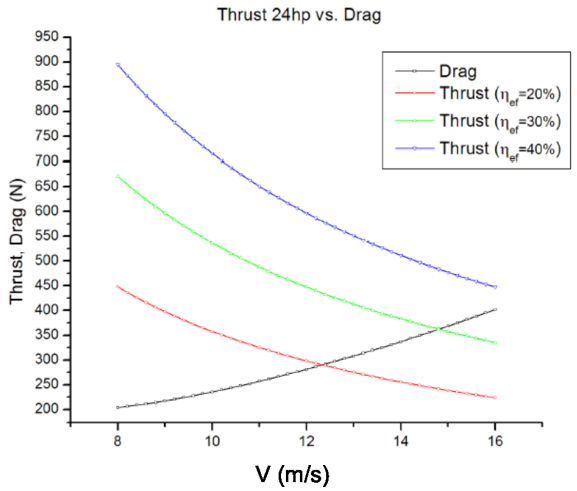

Fig. 9 Drag dependence with velocity and 24 hp engine available thrust curves.

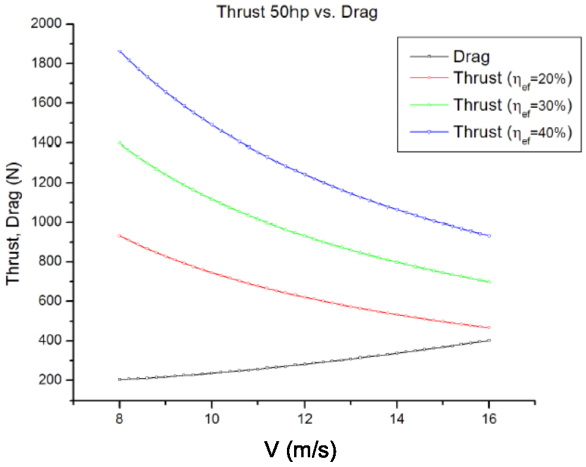

Fig. 10 Drag dependence with velocity and 50 hp engine available thrust curves.

The propulsive analysis with the 24 hp engine, shown in Fig. 9, indicates that fight is viable with this engine, but only under very restrictive conditions. For instance, according to these curves, the maximum possible flight speed would be just a little over 12 m/s, if the 20 % efficiency curve is used. However, as already pointed out, the drag results here obtained are probably lower than the actual drag in flight due to the geometric simplifications adopted. Therefore, the drag curves in Figs. 9 and 10 should be shifted upward, further restricting the admissible flight speed range. As also already pointed out, the power deficiency of the 24 hp engine became evident in September 1906 during a flight attempt, when the aircraft, in spite of some jumps, was unable to take-off. The current analysis clearly indicates that, with the 50 hp engine, the propulsive restrictions are overcome, as the historical accounts report.

Another aspect that should be mentioned is the fact that, during take-off, the ground causes additional drag forces. On the other hand, there are also lift increments due to ground effect. An initial analysis of ground effect is presented in Fig. 11, in which the influence of the distance to the ground in both airplane lift and drag coefficients is indicated. One can see in this figure that, as the aircraft approaches the ground, lift increases faster than drag. This behavior can justify the hoping-type flight observed on the September 1906 flight attempts. It is clear, however, that a more detailed analysis of all these effects is necessary in order to better quantify the influence of all parameters involved.

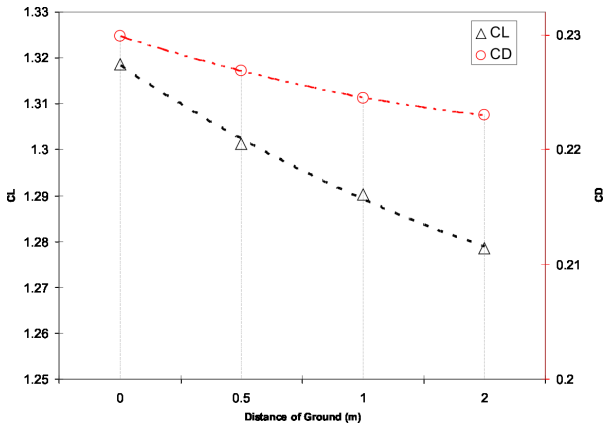

Fig. 11 Ground effect influence.

5.2 Stability Analysis

Stability is possibly the most critical part of the 14-Bis aircraft flight due to the complex canard-biplane configuration. The canard function is to generate enough lift to compensate the moment caused by the wing-CG distance. The canard surface is placed well ahead of the center of gravity, creating an extensive de-stabilizing influence. Consequently, it was vital that, despite the forward motion of the neutral point due to the canard lift contribution, the aircraft CG position is still situated ahead of aircraft neutral point for longitudinal static stability.

The exact center of gravity position of the 14-Bis aircraft is unknown [4]. Therefore, conclusions concerning the aircraft stability are based on estimates of such CG position obtained from the observation of photos of tests Santos Dumont performed in which he hanged the aircrat presumably by the center of gravity. The stability criterium states that an airplane is stable if, when perturbed from its equilibrium condition, restorative moments bring the airplane back to the equilibrium condition. Therefore, based on the cited historical photos and according to an estimation of the mass of each airplane component, it is possible to find a range for the CG position which indicates that it must be situated between 7.0 and 7.5 m from the aircraft nose.

The test cases here considered explore the flight conditions in which the airplane has a linear aerodynamic behavior, *i.e.*, the aerodynamic coefficients change linearly with the AoA and canard deflections. The resultant aerodynamic coefficients and derivatives for the aircraft and canard are listed in Table 3. For higher or lower angles, unsteady solutions were found in the present investigation. Another aspect that should be pointed out is the wing incidence angle, with regard to the fuselage, of approximately 5 deg. used in the 14-Bis aircraft. The authors further note that all moment coeffcients are calculated using

the CG as the reference point and the canard is kept with zero deflection for such calculations.

Table 3 Aerodynamic coefficients and derivatives of the airplane and control surfaces.

Aircraft		Canard	
$C_{L\alpha}$	4.85	$C_{L\delta_p}$	0.45
$C_{M\alpha}$	0.85	$C_{M\delta_p}$	1.31
C_{M_0}	-0.21		
C_{L_0}	0.85		

The present numerical results indicate that the 14-Bis aircraft would have an unstable condition in pitch for CGs situated farther than 6.87 m from the aircraft nose. Therefore, the results are showing that the 14-Bis was an unstable airplane, if the current estimated range for CG positions is right. Nevertheless, the authors emphasize that unstable airplanes can fly, despite the more difficult controlability. Moreover, it is also possible that Santos Dumont changed the CG position by adding weights. In any event, the current results are indicating that pitch static stability, and hence controlability, of the 14-Bis aircraft was certainly an issue. Furthermore, even if the plane were stable, small variations on the CG position could make it dangerously approach an unstable flight condition.

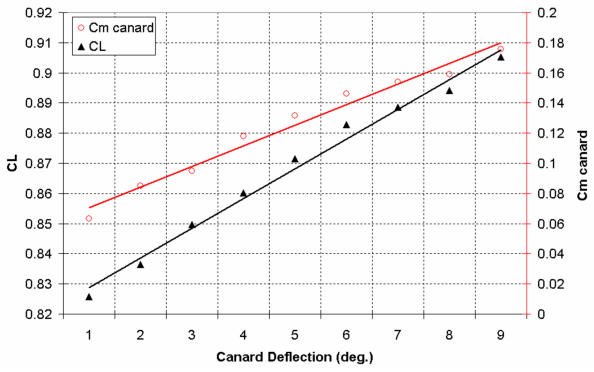

Fig. 12 $C_L \times \delta_p$ and $C_M \times \delta_p$ curves for the canard.

The plots in Fig. 12 present further information about the aerodynamic performance of the 14-Bis aircraft. Furthermore, the relative values of $C_{M\delta_p}$ and $C_{M\alpha}$, and of $C_{L\delta_p}$ and $C_{L\alpha}$ indicate that the canard seems to be effective to perform his principal function, which is the aircraft pitch control. However, since the aircraft resultant moment increases with the angle of attack, the airplane is unstable and the pilot would have to do more work to keep the airplane trimmed. The downwash effect of canard over the wing was also checked and, as expected, negligible effects were detected. This evidence leads the authors to discard the effect of the canard over the wing. Moreover, it is interesting to observe that the canard generates approximately 9.7 N of lift, without deflection, even though the canard is modeled as flat plates. This effect is not noticeable in terms of the total lift, but a significant pitch moment is added due to the canard position well ahead of the aircraft CG position.

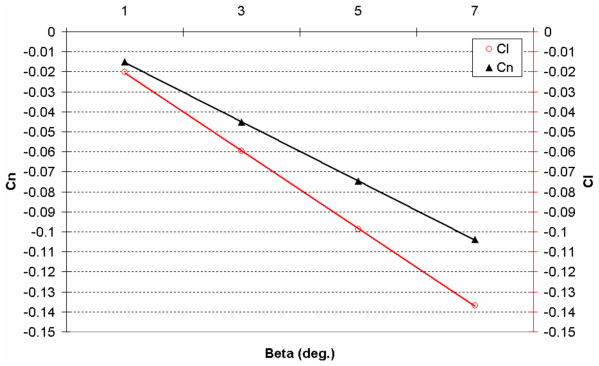

Fig. 13 $C_\ell \times \beta$ and $C_n \times \beta$ curves for the aircraft.

The influence of lateral flow on the airplane is studied by varying the sideslip angles. The results in Fig. 13 indicate that the linear approximation for the lateral stability derivatives seems perfectly reasonable. As can be observed, the sideslip angle induces significant and equally important roll and yaw moments, since both coefficients have the same order of magnitude. This points out a coupling between roll and yaw moments, which is an underlying characteristic of the airplane. The numerical results have also shown that the lateral flow has negligible influence on the longitudinal coefficients C_L and C_D, causing a maximum relative variation of 3 % in

these coefficients within the sideslip angle range tested.

6 Conclusion

The present work has used CFD techniques to perform an aerodynamic evaluation of the 14-Bis aircraft configuration. The historical flight conditions are simulated using a finite volume method and solving the RANS equations with the Menter SST turbulence model. A geometrically simplified model of the aircraft is used and the results obtained so far seem to corroborate many of the historical reports.

The results presented in the previous section confirm that the 24 hp power engine would probably yield an underpowered aircraft, thus making the 14-Bis unable take off during the first flight attempt on September 1906. Therefore, the engine change, selecting a more powerful one with 50 hp, is clearly justified. Based on the present calculations, it is difficult to believe that 11 m/s was the true airspeed of the aircraft, because the lift vs. speed curve, that was generated during the simulations, indicates very restrictive conditions concerning such flight speed. An acceptable speed, assuming a 5 deg. angle of attack, seems to be between 12 m/s and 14 m/s. These speeds could be reached more easily when flying against the wind direction. In any event, it can be stated, based upon the present numerical results, that the flight speeds should have been higher than 12 m/s.

A well defined range of flight conditions was found, namely AoA between 5 and 10 deg., canard deflection between -5 and 5 deg. and flight speeds between 11 and 14 m/s. This indicates that the flight conditions are, in fact, wider than the historical values usually cited. Other important aircraft characteristics were identified, as the roll and yaw coupling when subjected to lateral flow.

The analysis of longitudinal static stability considered the linear regime and it has shown that the position of the neutral point estimated is coherent with the reality of historical reports. Moreover, the parametric tests demonstrated that small center of gravity position variations, around the historical point, could make the aircraft statically unstable.

References

[1] Vilares, H. D., *Quem Deu Asas ao Homem*, Instituto Nacional do Livro, Rio de Janeiro, 1956.

[2] Menter, F.R., "Two-Equation Eddy-Viscosity Turbulence Models for Engineering Applications," *AIAA Journal*, Vol. 32, No. 8, Aug. 1994, pp. 1598-1605.

[3] CFX, www.waterloo.ansys.com/cfx/, 2005.

[4] Greco, P.C., and Ribeiro, M.L., *A Study of the Aerodynamic, Stability and Control Characteristics of the 14-Bis Aircraft*, Technical Report FAPESP No. 01/11158-7, Escola de Engenharia de São Carlos, Universidade de São Paulo, São Carlos, 2003 (in Portuguese, original title is *Estudo das Características Aerodinâmicas, de Estabilidade e de Controle do 14-Bis*).

[5] ICEMCFD, http://www.icemcfd.com/icemcfd.html, 2005.

[6] Field, D.A., "Laplacian Smoothing and Delaunay Triangulations," *Communications of Applied Numerical Methods*, Vol. 4, 1987, pp. 709-712.

[7] van der Vooren, J., and Slooff, J.W., "CFD Based Drag Prediction: State-of-the-Art Theory and Prospects," National Aerospace Laboratory, TP 90247L, The Nederlands, Aug. 1990.

Acknowledgments

The authors are indebted to Prof. Paulo Greco, from Escola de Engenharia de São Carlos, Universidade de São Paulo, who provided the geometrical CAD model, and to Mr. Marcus Reis, from Engineering Simulation and Scientific Software, ESSS, who provided support and licences for all used software. The authors also acknowledge the partial support of Conselho Nacional de Desenvolvimento Científico e Tecnológico, CNPq, through the Integrated Project Research Grants No. 501200/2003-7 and 502053/2004-6.